Spectrochimica Acta Part A: Molecular and Biomolecular Spectroscopy 152 (2016) 8–17

Contents lists available at ScienceDirect

Spectrochimica Acta Part A: Molecular and Biomolecular Spectroscopy

journal homepage: www.elsevier.com/locate/saa

Synthesis and spectroscopic characterization on 4-(2,5-di-2-thienyl-1H-pyrrol-1-yl) benzoic acid: A DFT approach

M. Kurt [a], E. Babur Sas [a], M. Can [b], S. Okur [c], S. Icli [d], S. Demic [c], M. Karabacak [e], T. Jayavarthanan [f], N. Sundaraganesan [g,*]

[a] Department of Physics, Ahi Evran University, Kırsehir, Turkey
[b] Department of Engineering Sciences, Faculty of Engineering, Izmir Katip Celebi University, Cigli, 35620 Izmir, Turkey
[c] Izmir Katip Celebi University, Material Science and Engineering, Cigli, Izmir, Turkey
[d] Ege University, Solar Energy Institute, 35040 Bornova, Izmir, Turkey
[e] Department of Mechatronics Engineering, H.F.T. Technology Faculty, Celal Bayar University, Turgutlu, Manisa, Turkey
[f] Department of Physics (Science and Humanities), Sri Manakula Vinayagar Engg. College, Madagadipet, Puducherry 605107, India
[g] Department of Physics (Engg.), Annamalai University, Annamalai Nagar 608 002, Tamil Nadu, India

HIGHLIGHTS

- The FT-IR spectra of 4-(2,5-di-2-thienyl-1H-pyrrol-1-yl) benzoic acid were recorded.
- The vibrational frequencies were calculated by DFT method and compared.
- NMR and MEP analysis were also carried out.
- UV–Vis spectra were recorded and compared with calculated ones.

GRAPHICAL ABSTRACT

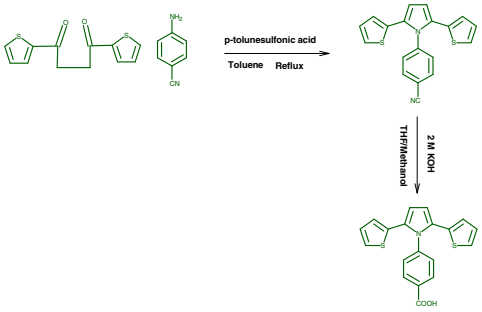

ARTICLE INFO

Article history:
Received 1 December 2014
Received in revised form 8 July 2015
Accepted 9 July 2015
Available online 10 July 2015

Keywords:
DFT
TPBA
Vibrational assignments
NBO
NMR
Thermodynamic properties

ABSTRACT

A complete structural and vibrational analysis of the 4-(2,5-di-2-thienyl-1H-pyrrol-1-yl) benzoic acid (TPBA), was carried out by ab initio calculations, at the density functional theory (DFT) method. Molecular geometry, vibrational wavenumbers and gauge including atomic orbital (GIAO) ^{13}C NMR and ^{1}H NMR chemical shift values of (TPBA), in the ground state have been calculated by using ab initio density functional theory (DFT/B3LYP) method with 6-311G(d,p) as basis set for the first time. Comparison of the observed fundamental vibrational modes of (TPBA) and calculated results by DFT/B3LYP method indicates that B3LYP level of theory giving yield good results for quantum chemical studies. Vibrational wavenumbers obtained by the DFT/B3LYP method are in good agreement with the experimental data. The study was complemented with a natural bond orbital (NBO) analysis, to evaluate the significance of hyperconjugative interactions and electrostatic effects on such molecular structure. By using TD-DFT method, electronic absorption spectra of the title compound have been predicted and a good agreement with the TD-DFT method and the experimental one is determined. In addition, the molecular electrostatic potential (MEP), frontier molecular orbitals analysis and thermodynamic properties of TPBA were investigated using theoretical calculations.

* Corresponding author.
E-mail address: sundaraganesan_n@yahoo.com (N. Sundaraganesan).

http://dx.doi.org/10.1016/j.saa.2015.07.058
1386-1425/

1. Introduction

The chemical properties of compounds containing aromatic carboxyl have been extensively investigated in the past decades. Pyrroles are components of more complex macrocycles, including the porphyrins of heme, the chlorins, bacteriochlorins, chlorophyll, porphyrinogens [1]. Pyrrole is a 5-membered aromatic heterocycle, like furan and thiophene. Unlike furan and thiophene, it has a dipole in which the positive end lies on the side of the heteroatom, with a dipole moment of 1.58 D [2]. Synthesized electroactive processable polymeric materials with a linear combination of thiophenes as the external units and N-substituted pyrrole as the central unit (2,5-di(2-thienyl)-1H-pyrrole derivatives) have attracted interest. Kim et al. [3] have been studied the synthesis, electrochemical, and spectroelectrochemical properties of conductive poly-[2,5-di-(2-thienyl)-1H-pyrrole-1-(p-benzoic acid)]. They investigated their study that the 2,5-di(2-thienyl)-1H-pyrrole derivative, [(2,5-di-(2-thienyl)-1H-pyrrole)-1-(p-benzoic acid)] (DPB) was chosen as a model compound. Because, in that particular system, the carboxylic acid group of benzoic acid is one of the most useful units to further incorporate functional groups into the polymer backbone. New type 2,5-di(2-thienyl)pyrrole derivative namely 4-amino-N-(2,5-di(thiophen-2-yl)-1H-pyrrol-1-yl)benzamide have been synthesized via reaction of 1,4-di(2-thienyl)-1,4-butanedione and p-aminobenzoyl hydrazide by Soyleyici et al. [4].

The calculations based on DFT method have been used in many areas [5–8]; the results are also in good agreement with the experimental results in calculating vibrational wavenumbers. In this study, we first synthesized 4-(2,5-di-2-thienyl-1H-pyrrol-1-yl) benzoic acid then the geometrical parameters, fundamental frequencies, electronic transitions, thermodynamic properties and GIAO ^{1}H and ^{13}C NMR chemical shifts of the TPBA molecule in the ground state have been calculated by using the DFT method with 6-311G(d,p) as basis set. In these DFT studies, the geometric structures of the TPBA molecule, i.e. bond lengths, bond angles, and torsion angles, have been calculated. We need experimental results to confirm the calculations; however, such experimental data are scarce. The crystal structure for the title molecule is not available; hence it is compared with the available experimental counterparts. Whereas, the comparison of the experimental and theoretical spectra reveals that very useful in making correct assignments and understanding the basic chemical shift-molecular structure relationship. And so, these calculations are valuable for providing insight into molecular analysis.

2. Synthesis

Synthesis of 1,4-dithiophene-2-yl-butane-1,4-dione (**1**). A solution of thiophene (9.61 mL, 0.12 mol) and $AlCl_3$ (16 g, 0.12 mol) in dry CH_2Cl_2 (50 mL) was added dropwise to a suspension of succinyl chloride (5.5 mL, 0.05 mol) in dry CH_2Cl_2 (50 mL) at 0 °C. The mixture was stirred for at 18–20 °C 4 h and poured into a mixture of 100 g ice and 10 mL hydrochloric acid and stirred for 1 h and the resulting dark green organic phase was washed with concentrated $NaHCO_3$ (3 × 25 mL), and dried over Na_2SO_4. After the solvent was evaporated, a blue–green solid remained and was suspended in ethanol. Column chromatography (SiO_2, CH_2Cl_2) and recrystallization from ethanol produced 8.98 g (68%) of it in a white solid. ^{1}H NMR: (400 MHz; $CDCl_3$): 7.80 (dd, 2H), 7.63 (dd, 2H), 7.13 (dd, 2H), 3.38 (s, 4H).

Synthesis of 4-(2,5-di-2-thienyl-1H-pyrrol-1-yl)benzonitrile (**2**): 4-Aminobenzonitrile (0.26 g, 2.2 mmol), 1,4-dithiophene-2-yl-butane-1,4-dione (1) (0.5 g, 2 mmol), and p-toluenesulfonic acid (6.8 mg, 0.4 mmol) in 30 ml dry toluene were heated under reflux in a Dean–Stark apparatus. After checking the completion of the reaction by TLC, it was set to cooling to room temperature, extracted with chloroform (3 × 25 mL) and water (3 × 25 mL). Then, the organic phase was dried over magnesium sulfate, and evaporated by rotary evaporator. The crude product was purified by column chromatography (dichloromethane) on silica gel to afford light brown colored product (72% yield). ^{1}H NMR ($CDCl_3$): 7.67 (d, 2H), 7.36 (d, 2H), 7.13 (d, 2H), 6.86 (t, 2H), 6.53 (s, 4H).

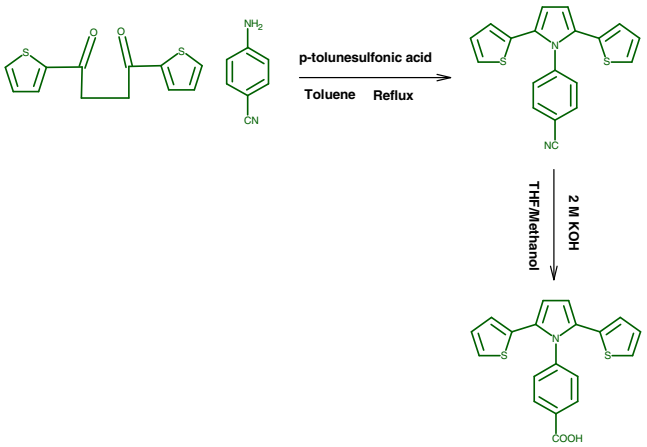

Fig. 1. Synthesis scheme of 4-(2,5-di-2-thienyl-1H-pyrrol-1-yl)benzoic acid (TPBA).

Synthesis of 4-(2,5-di-2-thienyl-1H-pyrrol-1-yl)benzoic acid (**3**): In a round bottomed flask an aqueous solution of potassium hydroxide (5 equiv., 2 N) was added to 2 (1 equiv.) dissolved completely in methanol and tetrahydrofuran (1:1) at 0 °C. Then, the solution was refluxed under argon atmosphere overnight with stirring. The reaction mixture was subjected to vacuum and crude product with ethyl acetate, the aqueous phase was acidified with 1 N HCl acid and subsequently extracted with ethyl acetate (3 × 25 ml). The combined organic layers were dried with sodium sulfate. Removal of the solvent provided the crude product of 3, which was then used without further purification. ^{1}H NMR (DMSO): 8.02 (d, 2H), 7.46 (d, 2H), 7.30 (d, 2H), 6.88 (t, 2H), 6.65 (d, 2H), 6.57 (s, 2H); Synthesis scheme of 4-(2,5-di-2-thienyl-1H-pyrrol-1-yl)benzoic acid has been shown in Fig. 1.

3. Experimental details

The compound TPBA in solid form were prepared using a KBr disc technique. The infrared spectrum of the compound was recorded in the range of 4000–600 cm^{-1} on a Perkin–Elmer FT-IR system spectrum BX spectrometer. The spectrum was recorded at room temperature, with a scanning speed of 10 cm^{-1} min^{-1} and the spectral resolution of 4.0 cm^{-1}. The ultraviolet absorption spectra of sample solved in DMSO was examined between 200 nm and 500 nm with resolution of 1 nm by Analytic JENA S 600 UV–Vis recording spectrometer. The sample spectrum was taken inside a quartz tupe with DMSO. NMR experiment was performed in Bruker DPX-400 at 300 K. Chemical shifts were reported in ppm relative to tetramethylsilane (TMS) for ^{1}H NMR spectrum in DMSO. NMR spectrum was obtained at the base frequency of 400 MHz for ^{1}H nuclei. The experimental HOMO–LUMO values for TPBA were calculated from cyclic voltammetry.

4. Computational details

The entire calculations were performed at Density functional theoretical (DFT) level with 6-311G(d,p) as basis set using Gaussian 03W [9] program package, invoking gradient geometry optimization [10]. Initial geometry generated from the standard geometrical parameters was minimized without any constraint on

the potential energy surface at HF level adopting the standard B3LYP/6-31G(d,p) basis set then re-optimized again at DFT level using the same basis set for better description. All the optimized structures were confirmed to be minimum energy conformations. Harmonic vibrational wavenumbers were calculated using analytic second derivatives to confirm the convergence to minima on the potential surface and to evaluate the zero-point vibrational energies (ZPVE). At the optimized structure of the TPBA, no imaginary frequencies were obtained, proving that a true minimum on the potential energy surface was found. By the use of potential energy distribution (PED) using VEDA 4 program [11] along with available related molecules, the vibrational frequency assignments were made with a high degree of accuracy. The natural bond orbital (NBO) calculations were performed using NBO 3.1 program [12] as implemented in the Gaussian 03W [9] package at the DFT/B3LYP level in order to understand various second order interactions between the filled orbitals of one subsystem and vacant orbitals of another subsystem, which is a measure of the intermolecular delocalization or hyperconjugation. The ^{1}H NMR isotropic shielding were calculated with the GIAO method [13,14] using the optimized parameters obtained from B3LYP/6-311G(d,p) method. The B3LYP method allows calculating the shielding constants with accuracy and the GIAO method is one of the most common approaches for calculating nuclear magnetic shielding tensors. The effect of solvent on the theoretical NMR parameters was included using the default model IEF–PCM provided by Gaussian 03W. The isotropic shielding values were used to calculate the isotropic chemical shifts δ with respect to tetramethylsilane (TMS).

5. Prediction of Raman intensities

The theoretical Raman intensity (I^R), which simulates the measured Raman spectrum, can be calculated using RAINT program [15]. The Raman activities (S_i) calculated by Gaussian 03 program [9] have been converted to relative Raman intensities (I^R). The theoretical Raman intensity (I^R), which simulates the measured Raman spectrum, is given by the equation [15,16]:

$$I_i^R = C(v_0 - v_i)^4 v_i^{-1} B_i^{-1} S_i \quad (1)$$

where 'B_i' is a temperature factor which accounts for the intensity contribution of excited vibrational states, and is represented by the Boltzmann distribution:

$$B_i = 1 - \exp\left(-\frac{h v_i c}{kT}\right) \quad (2)$$

In Eq. (1) 'v_0' is the frequency of the laser excitation line (in this work, we have used the excitation frequency $v_0 = 9398.5\ cm^{-1}$, which corresponds to the wavelength of 1064 nm of a Nd:YAG laser), 'v_i' is the frequency of normal mode (cm^{-1}), while 'S_i' is the Raman scattering activity of the normal mode Q_i. I_i^R is given in arbitrary units (C is a constant equal 10^{-12}). In Eq. (2) h, k, c, and T are Planck and Boltzmann constants, speed of light and temperature in Kelvin, respectively. Thus, the presented theoretical Raman intensities have been computed assuming 'B_i' equal to 1. The simulated spectra were plotted using a Lorentzian band shape with a half-width at half-height (HWHH) of 3 cm^{-1}.

6. Results and discussion

6.1. Molecular geometry

The optimized molecular structures obtained from GaussView program [17] are shown in Fig. 2. The most relevant structural parameters, bond lengths, bond angles and dihedral angles for TPBA have been employed without symmetry constraint by

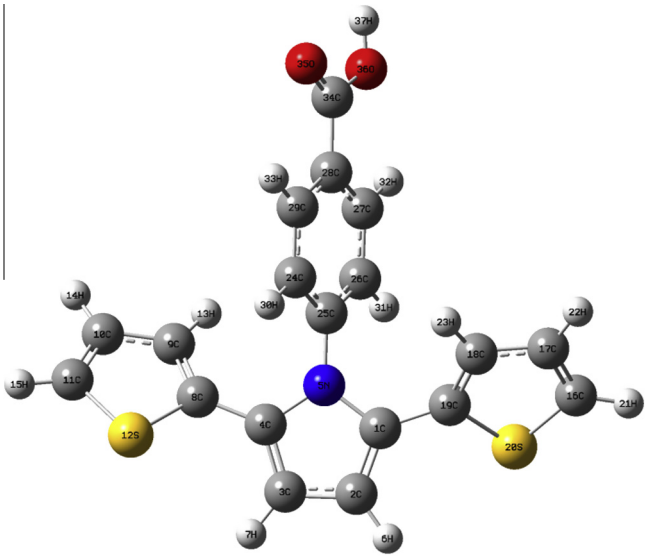

Fig. 2. Theoretical optimized geometric structure of the TPBA.

DFT/B3LYP method with the 6-311G(d,p) as basis set are presented in Tables SI-1 and SI-2 (Supplementary information). The TPBA molecule consists of two thiophene ring and benzoic acid structure substituted with pyrrole ring. The DFT calculation predicts the tilting around 41° between the thiophene rings and pyrrole ring. On the other hand, the benzoic acid exhibits the tilting around 62° with pyrrole ring. This shows the non-planarity of the entire molecule and also the individual planarity of the each rings.

The title molecule is considered to possess C_1 point group symmetry. The global minimum energy of TPBA was calculated at -1733.7013 Hartree. The C—S bond lengths in the thiophene rings are calculated at B3LYP/6-311G(d,p) level are 1.754 and 1.732 Å, respectively, which are smaller than the bond length of the single C—S bond (1.82 Å). The bonds, which act a bridge role between the thiophene rings and pyrrole ring are induced the C—S bond distances to the elongation of 1.754 Å whereas another values are calculated at 1.732 Å. The reported C—S bond distances values 1.759, 1.746 Å [18] 1.739 Å [19,20] 1.751 Å [21] are in agreement with calculated values. In the case of C—N bonds, The C1—N5 and C4—N5 bond distances are all calculated at 1.396 Å whereas the C25—N5 bond distance has been calculated at 1.428 Å at B3LYP/6-311G(d,p) level of theory which are shorter than that of normal C—N bond (1.47 Å) and longer than that of C=N bond (1.33 Å) [22]. But the second one is much closer to that of C—N bond distance [22].

The C—C bond length in benzene ring is between 1.388 and 1.399 Å at B3LYP/6-311G(d,p) level, which is much shorter than the typical C—C single bond (1.54 Å) and longer than the C=C double bond (1.34 Å) [23]. All the internal C—C—C bond angles in the benzene ring have been calculated around ~120° whereas in the thiophene ring which are calculated at around ~113°. The C—S—C bond angles are calculated at 91.8° which are in good agreement with the literature value of 92.1° [18]. It can be concluded from the calculated values, the geometrical parameters are slightly overestimated from the experimental values those are taken to be compared, due to the fact that the experimental results belong to the solid phase and theoretical calculations belong to isolated molecule in gas phase.

6.2. Vibrational assignments

Vibrational spectral assignments have been performed based on the recorded FT-IR spectra and the theoretically predicted

Table 1
Comparison of the calculated and experimental vibrational spectra and proposal assignments of TPBA.

No.	Exp. wavenumber	Theoretical wavenumber				Assignments (PED)
	FT-IR	Scaled	I_{IR}[a]	S_{Ra}[a]	I_{Ra}[a]	
1	3650	3647	106.78	197.57	3.01	υOH(100)
2		3144	0.34	155.40	2.89	υCH(97)
3		3139	0.56	255.24	3.67	υCH(97)
4		3138	0.56	265.11	3.71	υCH(98)
5		3130	5.66	69.06	0.20	υCH(98)
6		3112	2.25	64.57	0.19	υCH(99)
7		3111	2.41	60.81	0.18	υCH(99)
8		3108	0.78	115.62	0.35	υCH(99)
9		3102	1.98	75.74	0.23	υCH(99)
10		3094	9.10	130.27	0.40	υCH(96)
11		3093	11.44	131.13	0.40	υCH(98)
12		3091	1.77	41.56	0.13	υCH(98)
13	3070	3089	1.35	20.84	0.06	υCH(97)
	2984					Overtone + combination
	2851					Overtone + combination
	2671					Overtone + combination
	2549					Overtone + combination
14	1674	1744	351.28	125.72	1.47	υCO(83)
15	1610	1594	90.21	269.34	3.73	υCC(67), δCCH(16)
16	1576	1567	9.62	29.22	0.42	υCC(71)
17		1555	8.72	23.22	0.34	υCC(72)
18	1518	1538	0.62	2631.04	38.86	υCC(73)
19		1493	28.04	15.08	0.24	δCCH(50), υCC(33)
20		1490	9.11	1.68	0.03	υCC(59), δCCH(22)
21		1459	0.02	3024.43	49.03	υCC(63)
22		1421	20.53	0.87	0.02	υCC(79)
23	1431	1410	11.03	44.02	0.76	υCC(69)
24		1395	27.53	4.65	0.08	υCC(35), δCCH(31)
25		1380	86.21	33.53	0.60	υCN(27), υCC(24)
26		1332	3.52	9.49	0.18	δCCH(27), υCC(22)
27	1355	1331	182.11	64.50	1.22	δOH[δCOH(32)], υCO(22), υCC(20)
28		1327	39.75	96.61	1.84	υCN(26), υCC(18), δCCH(11)
29		1301	5.47	0.58	0.01	υCC(34), υCN(26)
30		1294	3.51	44.76	0.89	υCC(42), δCCH(19)
31	1286	1290	4.40	0.16	0.00	δCCH(51), υCC(24)
32		1272	1.09	1.68	0.03	δCCH(33), υCC(25), υCN(14)
33		1234	0.31	102.80	2.21	υCC(41), υCN(18)
34	1222	1225	7.59	15.40	0.33	δCCH(46)
35	1199	1197	4.88	16.01	0.36	δCCH(46), υCC(26)
36	1164	1172	31.11	1.51	0.03	δCCH(52), υCC(24)
37	1164	1172	138.06	29.05	0.68	δCCH(59), υCC(28)
38	1129	1149	163.63	64.20	1.55	δCCH(53), υCC(19)
39	1101	1096	3.29	1.79	0.05	δCCH(52), υCC(23)
40		1081	20.63	6.02	0.16	δCCH(32)
41		1072	28.11	19.63	0.53	δCCH(44), δCHS(14), υCC(10)
42		1070	123.88	6.65	0.18	δCCH(24), υCC(19)
43		1057	7.32	5.30	0.15	υCC(21), δCCH(18), δCHS(15)
44	1043	1040	0.77	3.31	0.09	υCC(47), δCCH(25)
45		1032	4.28	3.81	0.11	δCCH(35), υCC(32)
46		1030	8.24	157.81	4.50	δCCH(55), υCC(26)
47	1019	1012	5.09	32.40	0.95	υCC(33)
48		998	6.47	3.66	0.11	δCCC(37), δCCH(21), υCC(14)
49		968	0.13	0.27	0.01	γCH[τCCCH(38)]
50	950	956	0.10	0.31	0.01	γCH[τCCCH(39)]
51		887	10.13	27.40	0.98	δCCN(20), δCCC(17)
52		885	1.71	2.99	0.11	γCH[τCCCH(11), τCHCH(60)], τCSCH(11)
53		884	4.81	5.13	0.18	γCH[τCCCH(10), τCHCH(53)]
54	863	869	1.26	5.05	0.19	δCCC(28), δCCH(10)
55		854	23.42	0.11	0.00	γCH[τCCCH(48), τCNCH(20)], τCCCO(11)
56	840	840	0.15	6.73	0.26	γCH[τCCCH(33), τCNCH(13)]
57	834	826	1.09	5.63	0.22	γCH[τCCCH(79), τCNCH(18)]
58		819	49.55	4.08	0.16	υCS(37), δCCS(14), δCCC(11)
59		818	23.27	76.00	3.05	υCS(40), δCCS(14), δCCC(11)
60		815	8.56	1.19	0.05	γCH[τCCCH(43), τCSCH(18), τHCCH(17)]
61		812	15.66	11.56	0.47	τCCCH(44), τCCHS(19), τCCHH(17)
62	782	771	47.50	1.11	0.05	τCCCO(27), τCCCH(15), τCOOH(12)
63		770	25.58	43.03	1.89	υCC(39), δCCC(10)
64	764	763	34.09	0.04	0.00	γCH[τCCCH(61), τCNCH(20)]
65		720	6.20	6.09	0.29	υCS(59), δCCC(21)
66		717	0.36	22.75	1.10	υCS(64), δCCC(21)
67		700	53.37	1.80	0.09	τCCCC(28), τCCCH(21), τCCCO(12)
68	695	675	62.74	5.75	0.30	γCH[τCCCH(46), τCSCH(38)]
69		674	62.24	6.67	0.36	δCCH(46), γCH[τCSCH(38)]

(*continued on next page*)

Table 1 (*continued*)

No.	Exp. wavenumber	Theoretical wavenumber				Assignments (PED)
	FT-IR	Scaled	I_{IR}[a]	S_{Ra}[a]	I_{Ra}[a]	
70		667	19.90	6.55	0.35	τCCCN(26), τCCHN(14)
71		663	27.28	13.68	0.75	δCOO(16)
72		643	7.01	13.55	0.77	τCCCN(12)
73		634	3.00	8.50	0.49	δCCS(16), υCS(15), δCCC(15)
74		619	2.31	0.78	0.05	δCCC(33)
75		617	7.04	31.17	1.88	δCCS(29), υCS(18)
76		596	7.42	2.44	0.15	γOH[τCCOH(29)], υCS(13), δCCN(10)
77		575	41.85	1.65	0.11	γOH[τCCOH(28)], τCOOH(13)
78		568	0.09	30.81	2.10	τCCCC(64), γCH[ΓCCCH(16)], τCCCS(22)
79		551	19.91	6.09	0.43	τCCCS(15), τCCCC(13)
80		511	4.83	1.25	0.10	δCCO(12), υCC(11)
81		497	2.82	1.65	0.13	τCCCS(23), δCCO(18)
82		491	1.59	3.02	0.25	τCCCS(18)
83		474	17.39	6.60	0.58	τCCCS(10)
84		455	11.00	1.78	0.17	δCCO(15)
85		409	1.34	6.50	0.72	τCCCC(64), γCH[τCCCH(23)]
86		404	1.01	2.48	0.28	υCC(24), δCCS(20), δCCC(16)
87		377	3.84	3.87	0.49	δCCC(19)
88		372	6.99	1.05	0.13	δCCN(23)
89		324	0.58	2.78	0.44	τCCCS(22), τCCCC(16)
90		288	2.27	4.37	0.83	δCCN(17), τCCCC(16), τCCCN(11), τCCCO(11)
91		258	0.71	1.85	0.41	δCCC(23), δCCS(18), τCCCN(13)
92		216	0.13	1.26	0.39	υCC(27), δCCS(15), υCN(11), υCS(11), δCCN(10)
93		207	0.26	4.70	1.53	δCCC(11)
94		185	1.29	1.02	0.39	δCCC(49), δCCO(16)
95		156	0.51	0.50	0.26	τCCCC(21), δCCN(16)
96		121	1.11	14.44	11.86	τCCCN(14), δCCS(14), δCCC(12), τCCCC(11), τCCSN(13)
97		115	0.14	0.59	0.54	δCCC(14), τCCCC(14), δCCN(11)
98		91	0.62	2.02	2.76	τCCCC(23), τCCCN(22), δCCN(10)
99		83	0.44	9.98	16.35	τCCCO(48), τCCCN(27)
100		66	0.74	2.62	6.52	τCCCO(26), δCCC(17), τCCCC(17), δCCN(13)
101		42	0.76	16.92	100.00	τCCCN(33), τCCCO(19), τCCCS(10)
102		40	0.15	0.40	2.60	τCCCN(30), τCCSN(24)
103		33	0.26	1.86	17.90	τCCCN(61)
104		28	0.59	6.37	82.95	τCCCN(47), τCCSN(19), τCCCS(16)
105		26	0.10	5.04	74.87	τCCNC(18)

[a] I_{IR}, infrared intensity; S_{Ra}, Raman activity; I_{Ra}, Raman intensity; υ, stretching; δ, in plane bending; γ, out of plane bending; τ, torsion.

wavenumbers of TPBA. The recorded FT-IR and calculated vibrational wavenumber along with their relative intensities and probable assignments of TPBA are given in Table 1. The experimental FT-IR and calculated Infrared and Raman spectra of the title molecule depicted as Fig. 3. Any discrepancy noted between the observed and the calculated frequencies may be due to the two facts: one is that the experimental results belong to solid phase and theoretical calculations belong to gaseous phase; the another one is that the calculations have been actually done on a single molecule contrary to the experimental values recorded in the presence of intermolecular interactions. It is customary to scale down the calculated harmonic frequencies in order to improve the agreement with the experiment. Vibrational frequencies calculated at B3LYP/6-311G(d,p) level of theory were scaled by 0.967 to correct the theoretical error in this work.

6.2.1. COOH group vibrations

The O—H group gives rise to the three vibrations viz., stretching, in-plane bending and out-of-plane bending vibrations. The O—H group vibrations are likely to be the most sensitive to the environment, so they show pronounced shifts in the spectra of the hydrogen-bonded species. In the case of unsubstituted phenol it has been shown that the frequency of O—H stretching vibration in the gas phase is 3657 cm^{-1} [24]. In the present study the broad bands observed in FT-IR spectrum at 3650 cm^{-1} is assigned to O—H stretching vibrations. The theoretical values at 3647 cm^{-1} in B3LYP method gives good agreement with the experimental wavenumber. The PED corresponding to this vibration is a pure stretching mode and it is exactly contributing to 100%.

Vibrational analysis of COOH group is made on the basis of C=O group and OH group. The most characteristic feature of the carboxylic group is a single band observed usually in the region 1740–1660 cm^{-1} [25]. In solid state most of the carboxylic acids exist in dimeric form because of the inter-molecular hydrogen bonding between two COOH groups. In such a case C=O stretching vibrations are expected, one in-phase (symmetric stretching vibration) is Raman active and other one out-of-phase (anti-symmetric stretching vibration) is IR active. Similarly in the present study also a very strong band observed in FT-IR at 1674 cm^{-1} is assigned C=O stretching vibration. But the theoretically computed value at 1744 cm^{-1} shows deviation of about 70 cm^{-1} when compared with their experimental counterpart and this deviation may be due to the presence intermolecular interaction. The carboxylic acid deformation vibrations are expected in a wide range of 1450–1150 cm^{-1} depending on whether the acid is monomeric or dimeric. In the present study the frequency observed at 1355 cm^{-1} in FT-IR spectra is assigned for deformation vibration. The theoretically computed values at 1331 cm^{-1} show good agreement with the experimental observations.

6.2.2. C—H vibrations

The existence of one or more aromatic rings in a structure is readily determined from the C—H and C=C—C ring related vibrations. The C—H stretching occurs above 3000 cm^{-1} and is typically exhibited as a multiplicity of weak to moderate bands compared with the aliphatic C—H stretch [26]. In this region the bands are not affected appreciably by the nature of substituent. From Table 1 the observed FT-IR spectral wavenumbers are assigned to

the C—H stretching modes of aromatic group of TPBA. The medium band in FT-IR at 3070 cm^{-1} is assigned to C—H stretching vibrations. The theoretically computed wavenumbers (mode Nos. 2–13) by B3LYP/6-311G(d,p) level of theory predicted at 3144, 3139, 3138, 3130, 3112, 3111, 3108, 3102, 3094, 3093 and 3091 cm^{-1} fall within the recorded spectral range. As expected these modes are pure stretching modes as it is evident from the Table 1.

The observed C—H in-plane bending vibrations are assigned at 1222, 1199, 1164, 1164, 1129 and 1101 cm^{-1} in FT-IR spectra. The wavenumbers are predicted at 1272, 1225, 1197, 1172, 1172, 1149, 1096, 1081, 1072, 1070, 1032 and 1030 cm^{-1} (mode Nos.31, 32 and 34–42, 45 and 46) for the same vibrations which also correlated with the experimental values. Furthermore, the band is observed at 950 cm^{-1} in FT-IR spectrum for out of plane bending vibrations. The calculated wavenumber values at 968, 956, 885, 884, 854, 840, 826 and 815 cm^{-1} for the out-plane-bending vibrations are found to be exactly correlated with their experimental counterpart.

6.2.3. C—S and C—N vibrations

In the case of thiophene two C—S stretching vibrations are attributed, one is fell in higher wavenumber and another one is in lower wavenumber. The C—S stretching wavenumbers are observed by Kwiatkowski et al. and Bak et al. [27,28] at 840 and 754 cm^{-1} whereas Kupka et al. [29] have been predicted theoretically at 842 and 750 cm^{-1} by DFT method. Notwithstanding the fact, in our present study, the ring connected C—S bond stretching vibrations predicted in lower wavenumber at 720 and 717 cm^{-1} whereas the another C—S bond stretching vibrations attributes in higher wavenumber at 819 and 818 cm^{-1}. The PED contributes around 60% in the lower wavenumber region whereas in the higher wavenumber region this contribution falls around 40% shown in the Table 1. The CS in-plane-bending vibrations are predicted at 634 and 617 cm^{-1} by B3LYP method. The deformation vibrations are also predicted in the lower wavenumber region at 497, 491, 474 and 324 cm^{-1} respectively. The other essential characteristic vibrations of the title compound is C—N stretching vibrations, which are predicted at 1380, 1327 and 1301 cm^{-1} in B3LYP/6-311G(d,p) level of theory. There are no bands observed in the experimental spectrum. The deformation vibrational wavenumbers of C—N group are observed at 840 and 834 cm^{-1} in FT-IR spectrum. The theoretically predicted C—N deformation vibrational wavenumbers are calculated at 887, 854, 840 and 826 cm^{-1} in B3LYP level. The PED column shows these modes are a mixed one with minor contributions.

6.2.4. C—C vibrations

The ring stretching vibrations are very much important in the spectrum of benzene, pyridine and their derivatives are highly characteristic of the aromatic ring itself. C—C ring stretching vibrations occur in the region 1430–1625 cm^{-1}. In general, the bands are of variable intensity and are observed at 1625–1590, 1575–1590, 1470–1540, 1430–1465 and 1280–1380 cm^{-1} from the wavenumber ranges given by Varsanyi [30] for the five bands in the region. In the present study, the C—C stretching vibrations are found at 1610, 1576, 1518 cm^{-1} in IR spectra for Benzene ring. The computed wavenumbers at 1594, 1567, 1555, 1538 and 1395 cm^{-1} by DFT method assigned C—C stretching vibrations for the Benzene ring. The band observed at 1431 cm^{-1} in IR spectra identified as C—C stretching vibrations for the pyrrole ring. These vibrations also computed at 1490, 1410 and 1380 cm^{-1} by DFT method for pyrrole ring. The band observed at 1043 cm^{-1} in IR spectra identified as C—C stretching vibrations for the thiophene ring. These vibrations also calculated at 1459, 1421, 1301, 1294, 1057 and 1040 cm^{-1} by DFT method for thiophene ring. The

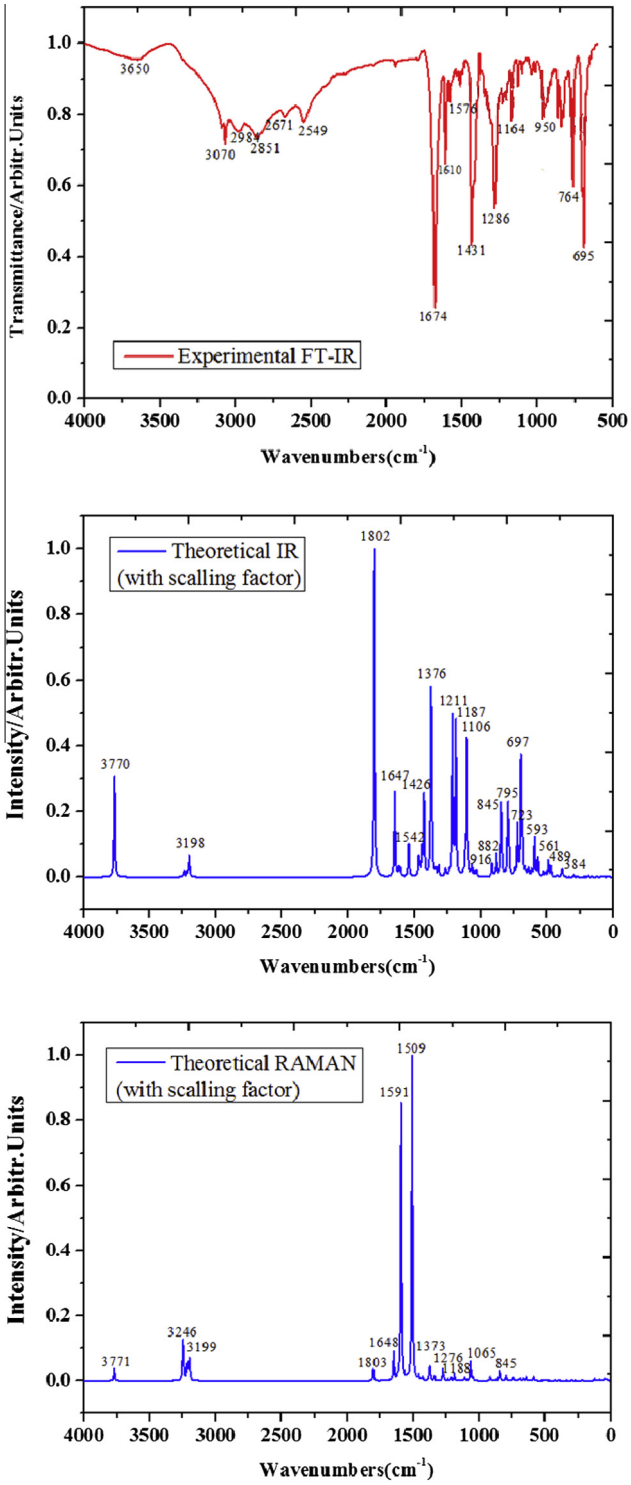

Fig. 3. The experimental FT-IR and calculated infrared and Raman spectra of the TPBA.

wavenumber 1234 cm^{-1} has also been assigned for C—C stretching vibrations which calculated by B3LYP/6-311G(d,p) level of theory. The C—C—C in-plane-bending bands always occur between the value 1000–600 cm^{-1} [31]. The band observed at 863 cm^{-1} in FT-IR spectrum is assigned to C—C—C deformations of phenyl ring. The computed wavenumbers at 998, 869, 619, 377, 207, 185 and 115 cm^{-1} by DFT method have been assigned C—C—C in plane bending vibrations. The PED contribution for this mode is a mixed

mode as it is evident from Table 1. The calculated wavenumber at 700, 568, 409, 156 and 91 cm^{-1} are assigned as C—C—C—C torsional vibrations for the title molecule.

6.3. ^{13}C and ^{1}H NMR spectral analysis

Application of the gauge-including atomic orbital (GIAO) [32] approach to molecular system was significantly improved by an efficient application of the method to the ab initio SCF calculations, using technique borrowed from analytic derivative methodologies. GIAO procedure is somewhat superior since it exhibits a faster convergence of the calculated properties upon extension of the basis set used. Taking into account the computational cost and the effectiveness of calculation, the GIAO method seems to be preferable from many aspects at the present state of this subject. On the other hand, the density functional methodologies offer an effective alternative to the conventional correlated methods, due to their significantly lower computational cost. The ^{1}H and ^{13}C chemical shifts are measured in DMSO solvent and are calculated in different solvents as depicted in Table 2. The isotropic chemical shifts are frequently used as an aid in identification of reactive organic as well as ionic species. It is recognized that accurate predictions of molecular geometries are essential for reliable calculations of magnetic properties. At first the full geometry optimization of TPBA was performed by using B3LYP/6-311G(d,p) level of theory. Then, GIAO ^{1}H and ^{13}C chemical shift calculations of the TPBA has been made by same method. The ^{1}H and ^{13}C NMR spectra of TPBA measured in DMSO solvent are shown in Table SI-3.

The result in Table 3 shows that the range of ^{13}C NMR chemical shift of typical organic molecule usually is >100 ppm [33,34] the accuracy ensures reliable interpretation of spectroscopic parameters. The signals for aromatic carbons were observed at 125.22–141.62 ppm in ^{13}C NMR spectrum for the title molecule, since those carbon atoms which belong to benzene ring. The calculated values for benzene ring carbon atoms also fall within the expected range of 131.32–149.97 ppm. The exception in the case of aromatic ring carbon chemical shift is observed which are 125.22 and 141.62 ppm due to the substitution of carboxylic acid group and pyrrole nitrogen respectively. The chemical shift values in the pyrrole ring connected carbon atoms of the thiophene ring are observed 144.52 and 144.38 ppm whereas the calculated one is at 133.68 ppm which gives good agreement with the experimental chemical shift values. The signals of the aromatic proton were observed at 7.43–8.02 ppm which shows good agreement with theoretical value of 7.27–8.24 ppm. The adjacent proton chemical shift values H6 and H7 in pyrrole ring are calculated at 6.57 and 6.57 ppm which are exactly correlated with the experimental values those are also observed at 6.57 ppm of each. This shows that the correlation between theory and experiment for the title compound is good. For ^{1}H and ^{13}C chemical shifts, the calculated values are also agreement with the experimental values.

Table 2
Experimental and calculated chemical shifts (ppm) of TPBA.

Atom	Calculated				Exp.
	Ethanol	Water	Gas	DMSO	DMSO
C34	168.65	168.72	166.98	168.70	166.73
C25	149.97	149.97	149.93	149.97	141.62
C8	144.54	144.51	144.98	144.52	133.68
C19	144.40	144.37	144.90	144.38	133.68
C29	135.81	135.78	136.20	135.79	130.36
C4	135.17	135.18	134.89	135.18	131.60
C1	135.12	135.14	134.77	135.14	131.60
C27	135.05	135.08	134.49	135.07	130.36
C26	134.16	134.19	133.52	134.18	130.36
C24	134.14	134.15	133.83	134.15	130.36
C11	132.58	132.65	131.53	132.63	129.60
C16	132.54	132.62	131.40	132.60	129.60
C28	131.31	131.33	131.18	131.32	125.22
C17	130.24	130.27	129.50	130.26	127.23
C10	130.19	130.22	129.47	130.21	127.23
C9	129.60	129.64	128.88	129.63	124.75
C18	129.55	129.59	128.84	129.58	124.75
C2	116.06	116.00	116.94	116.02	110.10
C3	116.03	115.98	116.90	116.00	110.10
H33	8.24	8.24	8.26	8.24	8.02
H32	8.20	8.20	8.08	8.20	8.00
H30	7.29	7.29	7.19	7.29	7.46
H31	7.26	7.27	7.13	7.27	7.43
H21	7.18	7.19	6.94	7.19	7.30
H15	7.18	7.19	6.95	7.19	7.29
H22	6.74	6.75	6.58	6.75	6.87
H14	6.74	6.75	6.58	6.75	6.87
H6	6.57	6.57	6.50	6.57	6.57
H7	6.57	6.57	6.50	6.57	6.57
H37	6.10	6.13	5.47	6.12	–
H13	5.85	5.85	5.72	5.85	6.65
H23	5.83	5.83	5.70	5.83	6.65

6.4. NBO analysis

By the application of the second-order donor–acceptor NBO energetic analysis, insight in the most important delocalization schemes was obtained. NBO analysis gives information about intra and intermolecular bonding and interactions among bonds, and also provides a convenient basis for investigating the interactions in both filled and virtual orbital spaces along with charge transfer and conjugative interactions in molecular system. The second order Fock matrix was carried out to evaluate the donor–acceptor interactions in the NBO analysis [35]. The change in electron density (ED) in the (σ^*, π^*) antibonding orbitals and $E(2)$ energies have been calculated by natural bond orbital (NBO) analysis [36] using DFT method to give clear evidence of stabilization originating from various molecular interactions. NBO analysis has been performed on TPBA using NBO 3.1 program as implemented in the Gaussian 03 W package at the DFT-B3LYP/6-311G(d,p) level of theory in order to elucidate intramolecular hydrogen bonding, intramolecular charge transfer (ICT) interactions and delocalization of π-electrons of the flavone ring. The hyperconjugative interaction energy was deduced from the second-order perturbation approach [37]. The interaction result is a loss of occupancy from the localized NBO of the idealized Lewis structure into an empty non-Lewis orbital. For each donor (i) and acceptor (j), the stabilization energy $E(2)$ associated with the delocalization $i \rightarrow j$ is estimated as

$$E(2) = \Delta E_{ij} = q_i \frac{F(i,j)^2}{\varepsilon_j - \varepsilon_i}$$

Some electron donor orbital, acceptor orbital and the interacting stabilization energy resulted from the second-order-micro-disturbance theory, where q_i is the donor orbital occupancy, ε_i and ε_j are diagonal elements and $F(i,j)$ is the off diagonal NBO Fock matrix element reported [38,39]. The larger the $E(2)$ value, the more intensive is the interaction between electron donors and electron acceptors, i.e. the more donating tendency from electron donors to electron acceptors and the greater the extent of conjugation of the whole system.

In the present study, the intramolecular hyperconjugative interactions are formed by the orbital overlap between bonding (C—C), (C—N) and anti-bonding (C—C), (C—N) and (C—O) orbital which results in intramolecular charge transfer (ICT) causing stabilization of the molecular system. These interactions are observed as an increase in electron density (ED) in (C—C), (C—N) and (C—O) antibonding orbital that weakens the respective bonds shown in the Table SI-4. A strong intramolecular hyperconjugative interaction

Table 3
The experimental and computed (TD-/B3LYP/6-311(d,p)) absorption wavelength λ (nm), excitation energies E (eV), absorbance and oscillator strengths (f) of TPBA.

DMSO			Water			Gas			Ethanol			Experimental	
λ (nm)	E (eV)	f	λ (nm)	E (eV)	f	λ (nm)	E (eV)	f	λ (nm)	E (eV)	f	λ (nm)	E (eV)
344.63 (62 → 63)	3.5976	0.0000	409.97 (91 → 92)	3.0242	0.0271	422.00 (91 → 92)	2.9380	0.0156	410.68 (91 → 92)	3.0190	0.0274	340.68	3.643
281.67 (60 → 63) (61 → 63)	4.4017	0.0730	329.69 (91 → 93)	3.7607	0.6886	325.22 (91 → 93)	3.8123	0.5913	330.15 (91 → 93)	3.7554	0.6954	269.92	4.598
258.52 (59 → 63) (60 → 63) (61 → 64)	4.7959	0.1744	310.97 (91 → 94) (91 → 95)	3.9870	0.0010	321.11 (91 → 94)	3.8612	0.0011	311.47 (91 → 94) (91 → 95)	3.9806	0.0011	203.54	6.098

of π-electrons with the greater energy contributions from C1—C2 → C3—C4 (18.75 kJ mol^{-1}), C18—C19 (10.18 kJ mol^{-1}); C3—C4 → C1—C2 (18.77 kJ mol^{-1}), C18—C19 (10.04 kJ mol^{-1} for the pyrrole ring, C8—C9 → C10—C11 (16.04 kJ mol^{-1}), C3—C4 (9.10 kJ mol^{-1}); C10—C11 → C8—C9 (14.71 kJ mol^{-1}); C16—C17 → C18—C19 (14.68 kJ mol^{-1}); C18—C19 → C1—C2 (9.19 kJ mol^{-1}), C16—C17 (16.07 kJ mol^{-1}) for thiophene rings of the molecule, while C24—C29 → C25—C26 (22.95 kJ mol^{-1}), C27—C28 (19.33 kJ mol^{-1}); C25—C26 → C24—C29 (17.92 kJ mol^{-1}), C27—C28 (22.85 kJ mol^{-1}); C27—C28 → C24—C29 (20.82 kJ mol^{-1}), C25—C26 (19.73 kJ mol^{-1}), C34—O35 (21.28 kJ mol^{-1}); for the benzene ring of the molecule.

6.5. Electronic properties

6.5.1. Absorption spectra

TD-DFT/B3LYP/6-311G(d,p) calculations have been performed to determine the low-lying excited states of TPBA On the basis of fully optimized ground-state structure. The calculated result involving the vertical excitation energies, oscillation strength (f) and wavelength are carried out and compared with measured experimental wavelength listed in Table 3. Typically, according to Frank–Condon principle, the maximum absorption peak λ_{max} corresponds in an UV–Vis spectrum to vertical excitation. TD-DFT/B3LYP/6-311G(d,p) level of theory predict one intense electronic transition for DMSO at 4.4017 eV (281.67 nm) with oscillator strength f = 0.073 is in good agreement with the measured experimental data DMSO (exp = 269.92 nm) shown in Fig. 4. All the structures allow strong π–π* and σ–σ* transition in the UV–Vis region with high extinction co-efficients. The π–π* transitions are expected to occur relatively at lower wavelength, due to the consequence of the extended aromaticity of the benzene ring. Natural bond orbital analysis also indicates that molecular orbitals are mainly compared of π atomic orbital so above electronic transitions are mainly derived from the contribution of π–π* bands.

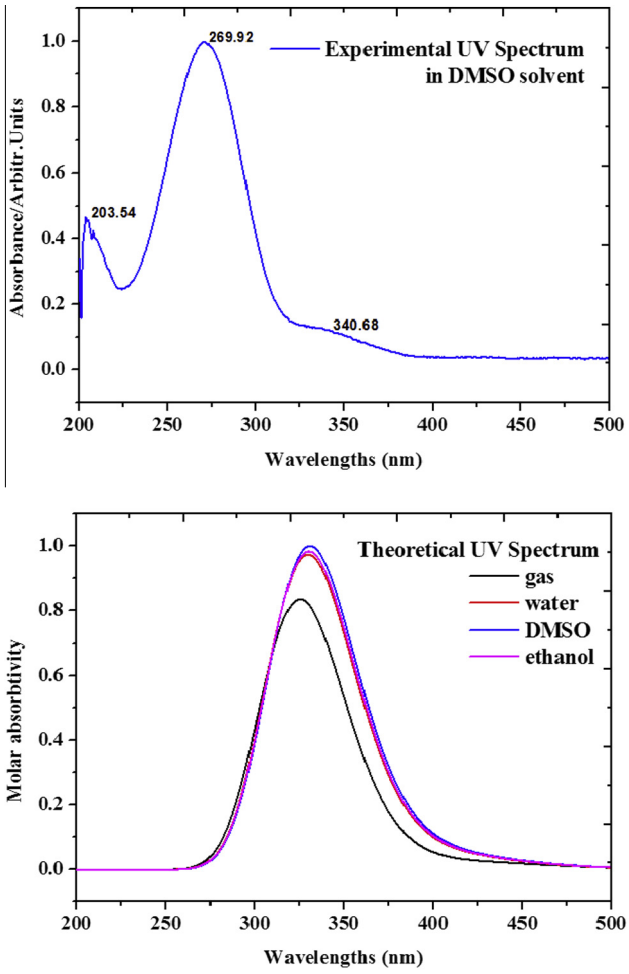

Fig. 4. The experimental (DMSO) and theoretical (gas, water, DMSO and ethanol) UV–Vis spectra of the TPBA.

6.5.2. Frontier molecular orbital analysis

The electronic absorption corresponds to the transition from the ground to the first excited state and is mainly described by one electron excitation from the highest occupied molecular orbital (HOMO) to the lowest unoccupied molecular orbital (LUMO). The HOMO represents the ability to donate an electron, LUMO as an electron acceptor represents the ability to obtain an electron. Both HOMO and LUMO are the main orbitals that take part in chemical stability [40]. The energy values of LUMO and HOMO and their energy gap reflect the chemical activity of the molecule. The decrease in the HOMO and LUMO energy explains the Intramolecular charge transfer (ICT) interaction taking place within the molecule which is responsible for the activity of the molecule. The HOMO–LUMO energy separation has served as a simple measure of kinetic stability. A molecule with a small or no HOMO–LUMO gap is a chemically reactive [41–43]. Pearson showed that the HOMO–LUMO gap represents the chemical hardness of the molecule [44,45]. The HOMO–LUMO energy gap of TPBA was calculated at the B3LYP/6-311G(d,p) level and their values shown below reveals that the energy gap reflect the chemical activity of the molecule. The HOMO is located over the thiophene and pyrrole rings of the molecule, the HOMO → LUMO transition implies an electron density transfer to benzoic acid from thiophene and pyrrole rings. Moreover, these orbital significantly overlap in their position for TPBA. The atomic orbital compositions of the frontier molecular orbital are sketched in Table SI-5. The calculated energy values in different solvent are shown in Table SI-6.

HOMO energy = −5.40 eV.
LUMO energy = −1.87 eV.
HOMO–LUMO energy gap = 3.53 eV.

Table 4
Thermodynamic properties at different temperatures at the B3LYP/6-311G(d,p) level for TPBA.

T (K)	C (cal mol^{-1} K^{-1})	S (cal mol^{-1} K^{-1})	H (kcal mol^{-1})
100	31.326	97.595	2.219
150	41.424	112.957	4.130
200	53.163	127.019	6.588
250	65.812	140.677	9.660
298.15	78.004	153.663	13.219
300	78.464	154.162	13.368
350	90.484	167.477	17.695
400	101.520	180.558	22.599
450	111.439	193.333	28.027
500	120.250	205.749	33.923
550	128.038	217.772	40.233
600	134.920	229.387	46.910
650	141.019	240.591	53.911
700	146.447	251.391	61.200

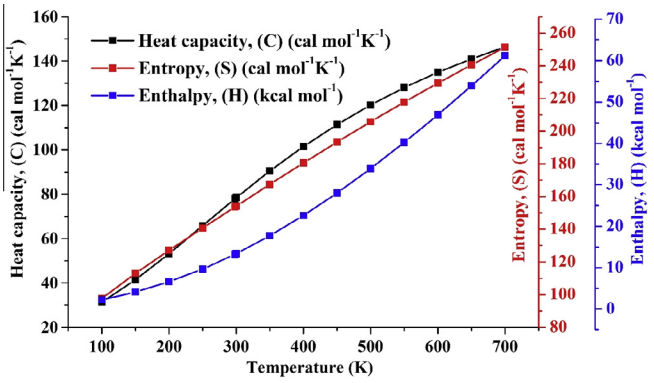

Fig. 5. The correlation graphic of heat capacity, entropy, enthalpy and temperature for TPBA molecule.

6.6. Molecular electrostatic potential (MEP) analysis

The molecular electrostatic potential (MEP) is related to the electronic density and is a very useful descriptor for determining sites for electrophilic attack and nucleophilic reactions as well as hydrogen-bonding interactions [46,47]. The molecular electrostatic potential, $V(r)$, at a given point $r(x, y, z)$ in the vicinity of a molecule, is defined in terms of the interaction energy between the electrical charge generated from the molecule electrons and nuclei and a positive test charge (a proton) located at r. To predict reactive sites for electrophilic and nucleophilic attack for the title molecule, MEP was calculated at the B3LYP/6-311G(d,p) optimized geometry. The negative (red) regions of MEP were related to electrophilic reactivity and the positive (white) regions to nucleophilic reactivity shown along with contour map in Table SI-7. The negative regions are mainly localized on the electronegative atoms. A maximum positive region is localized on the carboxylic acid group of the molecule indicating a possible site for nucleophilic attack. The electrophilic and nucleophilic sites give information about the region from where the compound can have non-covalent interactions.

6.7. Mulliken atomic charge

The Mulliken atomic charges of TPBA molecule calculated by DFT method at 6-311G(d,p) basic set in gaseous phase are given in Table SI-8. The charge distribution on the molecule has an important role in the application of quantum mechanical calculations for the molecular system. The charges at the sites of the C atom attached to the O atom are positive because of the electron-withdrawing nature of the O and N atoms. Due to strong negative charges of O atom, C34 accommodate positive charge and become more acidic. Other C atoms are negative. Moreover, Mulliken atomic charges also show that all the hydrogen atoms have a net positive charge but H37 atoms accommodate more positive atomic charges 0.257, than the other hydrogen atoms and is acidic. This is due to the presence of electronegative oxygen atoms (O35 and O36). The negative values of atomic charges of C atom in the aromatic ring lead to a redistribution of electron density.

6.8. Thermodynamical properties

On the basis of Vibrational analysis, the statistical thermo chemical analysis of TPBA is carried out by B3LYP/6-311G(d,p) level of theory considering the molecule to be at room temperature of 298.15 K and 1 atm pressure. The thermodynamic functions, like heat capacity (C), enthalpy changes (H) and entropy (S), rotational constants and zero point vibrational energy (ZPVE) of the molecule by DFT method for the title molecule were obtained from the theoretical harmonic frequencies and listed in Table SI-9. It can be observed that these thermodynamic functions such as heat capacity (C), enthalpy changes (H) and entropy (S), are increasing with temperature ranging from 100 to 700 K due to the fact that the molecular vibrational intensities increase with temperature which are shown in Table 4. The correlation equations between heat capacity, enthalpy changes, entropy and temperatures were fitted by correlation coefficients. The corresponding correlation graphics are shown in Fig. 5. All the thermodynamic data give helpful information for the further study on the title molecule.

7. Conclusion

The spectroscopic techniques such as FT-IR, NMR and UV–visible supported by the recent development of computational tool such as DFT method allow the structural analysis of our title molecule to be conducted in a seamless way. In the present study, the experimental approach to molecular properties has been shown by some examples of FT-IR, NMR and UV–visible spectroscopy. The theoretical support has been addressed by example of DFT/B3LYP/6-311G(d,p) calculations, and the peculiarities and limitations of the theoretical approach to the analysis have been considered. The good agreement between the experimental results and calculated frequencies indicate that the density functional methods provide valuable information for understanding the vibrational spectra of the TPBA molecule. NBO analysis gives the information about intermolecular and intra molecular charge transfer within the molecule. The UV–visible spectrum was also recorded and the energies of frontier MO's and the λ_{max} of the compound were also determined from TD-DFT method. The relative stabilities, HOMO–LUMO energy gap and implications of the electronic properties are examined and discussed. The observed and the predicted isotropic chemical shifts are found to be in good agreement. Thermodynamic properties in the range from 100 to 700 K are obtained. The gradients of heat capacity, entropy and enthalpy with temperature are always positive.

Appendix A. Supplementary data

Supplementary data associated with this article can be found, in the online version, at http://dx.doi.org/10.1016/j.saa.2015.07.058.

References

[1] J. Jusélius, D. Sundholm, Phys. Chem. Chem. Phys. 2 (2000) 2145–2151.
[2] <https://en.wikipedia.org/wiki/Pyrrole>.
[3] Yung Hyun Kim, Jaeyoung Hwang, Jung Ik Son, Yoon-Bo Shim, Synth. Met. 160 (2010) 413–418.

[4] Hakan Can Soyleyici, Metin Ak, Yüksel Şahin, Dilek Odacı Demikol, Suna Timur, Chem. Phys. 142 (2013) 303–310.
[5] Amitesh Maiti, Alexei Svizhenko, M.P. Anantram, Phys. Rev. Lett. 88 (2002) 1268051.
[6] Danhong Zhou, Ding Ma, Yan. Wang, Xianchun Liu, Xinhe Bao, Chem. Phys. Lett. 373 (2003) 46–51.
[7] J. Leconte, A. Markovits, M.K. Skalli, C. Minot, A. Belmajdoub, Surf. Sci. 497 (2002) 194–204.
[8] Jian-guo Wang, Chang-jun Liu, Zhiping Fang, Yue Liu, Zhongqi Han, J. Phys. Chem. B 108 (2004) 1653–1659.
[9] Gaussian 03W, Gaussian Inc.: Wallingford, 2004.
[10] H.B. Schlegel, J. Comput. Chem. 3 (1982) 214–218.
[11] M.H. Jamroz, Vibrational Energy Distribution Analysis, VEDA 4 Computer Program, Poland, 2004.
[12] E.D. Glendening, A.E. Reed, J.E. Carpenter, F. Weinhold, NBO Version 3.1, TCI, University of Wisconsin, Madison, 1998.
[13] R. Ditchfield, J. Chem. Phys. 56 (1972) 5688–5691.
[14] K. Wolinski, J.F. Hinton, P. Pulay, J. Am. Chem. Soc. 112 (1990) 8251–8260.
[15] D. Michalska, R. Wysokinski, Chem. Phys. Lett. 403 (2005) 211–217.
[16] S. Shen, G.A. Guirgis, J.R. Durig, Struct. Chem. 12 (2001) 33–43.
[17] A. Frisch, A.B. Nielson, A.J. Holder, GAUSSVIEW User Manual, Gaussian Inc, Pittsburgh, PA, 2000.
[18] Li Xiao-Hong, Liu Xiang-Ru, Zhang Xian-Zhou, Comput. Theor. Chem. 969 (2011) 27–34.
[19] A. Dolmella, S. Gatto, E. Girardi, G. Bandoli, J. Mol. Struct. 513 (1999) 177–199.
[20] S. Kikionis, V. Mckee, J. Markopoulos, O. Igglessi-Markopoulou, Tetrahedron 64 (2008) 5454–5458.
[21] O.R. Pons, L.S. Andrés, D. Burget, P. Jacques, J. Photochem. Photobiol. A Chem. (2006) 298–304.
[22] H.S. Chen, Z.M. Li, X.P. Yang, H.G. Wang, X.K. Yao, China Struct. J. Chem. 19 (2000) 317–325.
[23] J.J. Nie, D.J. Xu, China Struct. J. Chem. 21 (2002) 165–167.
[24] G. Varsanyi, Assignments for Vibrational Spectra of Seven Hundred Benzene Derivatives, vol. 1–2, Adam Hilger, 1974.
[25] D.L. Vein, N.B. Colthup, W.G. Fateley, J.G. Grasselli, The Handbook of Infrared and Raman Characteristic Frequencies of Organic Molecules, Academic Press, San Diego, 1991.
[26] J. Coates, in: R.A. Meyers (Ed.), Interpretation of Infrared Spectra: A Practical Approach, John Wiley and Sons Ltd., Chichester, 2000.
[27] J.S. Kwiatkowski, J. Leszczynski, I. Teca, J. Mol. Struct. 436–437 (1997) 451–480.
[28] B. Bak, D. Christensen, L. Hansen-Nygaard, J. Rastrup-Andersen, J. Mol. Spectrosc. 7 (1961) 58–63.
[29] T. Kupka, R. Wrzalik, G. Pasterna, K. Pasterny, J. Mol. Struct. 616 (2002) 17–32.
[30] G. Varsanyi, Vibrational Spectra of Benzene Derivatives, Academic Press, New York, 1969.
[31] A. Fu, D. Du, Z. Zhou, Spectrochim. Acta 59 (2003) 245–253.
[32] R. Ditchfield, Molecular orbital theory of magnetic shielding and magnetic susceptibility, J. Chem. Phys. 56 (1972) 5688–5691.
[33] H.O. Kalinowski, S. Brawn, Carbon13 NMR Spectroscopy, John Wiley and Sons, Chichester, 1988.
[34] K. Pinlajer, E. Kleinpeter (Eds.), Carbon13 Chemical Shifts in Structure and Spectrochemical Analysis, VCH publishers, Deerfield Beach, 1994.
[35] M. Sarafran, A. Komasa, E.B. Adamska, J. Mol. Struct. (Theochem.) 827 (2007) 101.
[36] H.W. Thomson, P. Torkington, J. Chem. Soc. 171 (1945) 640–645.
[37] E.D. Glendening, J.K. Badenhoop, A.E. Reed, J.E. Carpenter, J.A. Bohmann, C.M. Morales, F. Weinhold, NBO 5.0, Theoretical Chemistry Institute, University of Wisconsin, Madison, 2001.
[38] C. James, A. AmalRaj, R. Reghunathan, I.H. Joe, V.S. JayaKumar, J. Raman Spectrosc. 37 (2007) 1381–1392.
[39] L.J. Na, C.Z. Rang, Y.S. Fang, J. Zhejiang Univ. Sci. 6B (2005) 584–589.
[40] R.G. Pearson, J. Org. Chem. 54 (1989) 1423–1430.
[41] J.I. Aihara, Phys. Chem. Chem. Phys. 2 (2000) 3121–3125.
[42] X. Liu, T.G. Schmalz, D.J. Klein, Chem. Phys. Lett. 188 (1992) 550–554.
[43] M.D. Diener, J.M. Alford, Nature (London) 393 (1998) 668–671.
[44] R.G. Pearson, Proc. Natl. Acad. Sci. U.S.A. 83 (1986) 8440–8441.
[45] R.G. Pearson, J. Am. Chem. Soc. 110 (1988) 2092–2097.
[46] E. Scrocco, J. Tomasi, Adv. Quantum Chem. (1979) 11–115.
[47] N. Okulik, A.H. Jubert, Internet Electron. J. Mol. Des. (2005) 4–17.